Article No. jmbi.1999.3390 available online at http://www.idealibrary.com on IDEAL® J. Mol. Biol. (2000) 295, 517–526

JMB

Polymerization and Structure of Nucleotide-free Actin Filaments

Enrique M. De La Cruz[1,2], Anna Mandinova[3], Michel O. Steinmetz[3] Daniel Stoffler[3], Ueli Aebi[3] and Thomas D. Pollard[1,2]*

[1]*Department of Cell Biology and Anatomy, Johns Hopkins University School of Medicine 725 North Wolfe Street Baltimore, MD 21205, USA*

[2]*The Salk Institute for Biological Studies, Structural Biology Lab, 10010 N. Torrey Pines Road, La Jolla, CA 92037, USA*

[3]*Biozentrum, M. E. Müller Institute for Structural Biology, University of Basel CH-4056, Basel Switzerland*

**Corresponding author*

Two factors have limited studies of the properties of nucleotide-free actin (NFA). First, actin lacking bound nucleotide denatures rapidly without stabilizing agents such as sucrose; and second, without denaturants such as urea, it is difficult to remove all of the bound nucleotide. We used apyrase, EDTA and Dowex-1 to prepare actin that is stable in sucrose and ~99% free of bound nucleotide. In high concentrations of sucrose where NFA is stable, it polymerizes more favorably with a lag phase shorter than ATP-actin and a critical concentration close to zero. NFA filaments are stable, but depolymerize at low sucrose concentrations due to denaturation of subunits when they dissociate from filament ends. By electron microscopy of negatively stained specimens, NFA forms long filaments with a persistence length 1.5 times greater than ADP-actin filaments. Three-dimensional helical reconstructions of NFA and ADP-actin filaments at 2.5 nm resolution reveal similar intersubunit contacts along the two long-pitch helical strands but statistically significant less mass density between the two strands of NFA filaments. When compared with ADP-actin filaments, the major difference peak of NFA filaments is near, but does not coincide with, the vacated nucleotide binding site. The empty nucleotide binding site in these NFA filaments is not accessible to free nucleotide in the solution. The affinity of NFA filaments for rhodamine phalloidin is lower than that of native actin filaments, due to a lower association rate. This work confirms that bound nucleotide is not essential for actin polymerization, so the main functions of the nucleotide are to stabilize monomers, modulate the mechanical and dynamic properties of filaments through ATP hydrolysis and phosphate release, and to provide an internal timer for the age of the filament.

Keywords: actin, nucleotide, polymerization, electron microscopy, 3-D reconstruction

Introduction

Nucleotide bound to the high affinity site on actin monomers stabilizes the protein (Asakura, 1961) and influences assembly of the protein into filaments (reviewed by Pollard & Cooper, 1986; Carlier, 1990). Bound ATP is hydrolyzed (Straub & Feuer, 1950) after incorporation of subunits into the polymer (Pardee & Spudich, 1981; Pollard & Weeds, 1984), most likely in a random fashion (Ohm & Wegner, 1994). Slow dissociation of phosphate after ATP hydrolysis (Carlier & Pantaloni, 1988) results in a conformational change (Orlova & Egelman, 1992) that destabilizes the filaments, yielding a higher critical concentration for assembly of ADP-actin due to slower association and faster dissociation of ADP subunits at the barbed end of filaments (Pollard, 1984, 1986).

Nucleotide-free actin (NFA) monomers denature rapidly and irreversibly in dilute buffers (Asakura,

Present addresses: E. M. De La Cruz, University of Pennsylvania School of Medicine, Department of Physiology, 3700 Hamilton Walk, Philadelphia, PA 19104, USA; M. O. Steinmetz, Novartis Pharma AG, Functional Genomics Areas, Protein Sciences, CH-4002 Basel, Switzerland.

Abbreviations used: NFA, nucleotide-free actin; S.D., standard deviation; CTEM, conventional transmission electron microscopy; STEM, scanning transmission electron microscopy; ADF, annular dark-field.

E-mail address of the corresponding author: pollard@salk.edu

0022-2836/00/030517–10 $35.00/0

1961) unless protected by high concentrations of sucrose (Kasai *et al*., 1965). Sucrose protection has permitted characterization of NFA monomers and determination of the kinetic mechanisms and affinities for nucleotide ($K_d \sim 1$ nM; De La Cruz & Pollard, 1995) and profilin (Vinson *et al*., 1998). The high affinity of actin for ATP makes it difficult to remove all of the ATP, even in the presence of EDTA (De La Cruz & Pollard, 1995), unless urea is included in the buffer (Kasai *et al*., 1965). Kasai *et al*. (1965) established that actin stripped of ATP in urea can polymerize, but newer methods of analysis make possible a more quantitative assessment of polymerization, ligand binding and structure.

Here we characterize the polymerization and structure of NFA filaments. Polymerization of NFA is more favorable than ATP-actin. NFA filaments differ only slightly from ADP-actin filaments in their structure and ability to bind rhodamine phalloidin. Although the nucleotide cleft is empty, these filaments do not bind εATP. We conclude that bound nucleotide is not required for polymerization.

Results

Preparation of nucleotide-free actin (NFA)

Two steps carried out in 50 % sucrose remove >99 % of the nucleotide bound to muscle actin (Table 1). Chelation of divalent cations reduces the affinity of actin for nucleotide, which remains in a rapid equilibrium with actin. Apyrase enzymatically hydrolyzes the dissociated nucleotide to AMP, depleting ATP and ADP available to bind actin. Previous methods without apyrase (Kasai *et al*., 1965; De La Cruz & Pollard, 1995) removed only ~80 % of bound ATP.

Polymerization of nucleotide-free actin

Actin free of bound nucleotide and divalent cation polymerizes spontaneously in 46-50 % sucrose upon addition of KCl (Figure 1(a)). NFA monomers also polymerize if simply warmed to room temperature in low salt buffer. At steady-state the pyrene fluorescence of polymerized NFA indicates that the critical concentration is near zero (0.06 μM, S.D. = ± 0.04 μM, $n = 5$) and lower than MgATP-actin (0.19 μM, S.D. = ± 0.11 μM, $n = 5$) in the same buffer. In agreement with Drenckhahn & Pollard (1986) and Fuller & Rand (1999), sucrose does not change the critical concentration for the

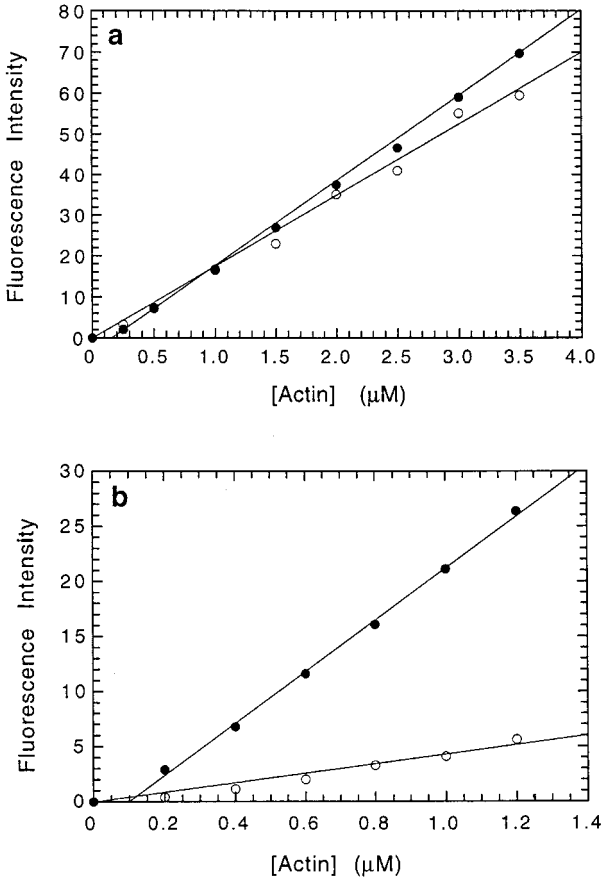

Figure 1. Steady-state polymerization of MgATP actin and NFA. Polymerization was assayed from the fluorescence of pyrene actin (5 %). Conditions: 50 mM KCl, 1 mM EGTA, 10 mM imidazole (pH 7.0), 0.5 mM DTT, 5 % pyrenyl-actin, 25 °C in (a) 46 % sucrose or (b) four hours after dilution of sucrose to 4.6 %. Samples of MgATP-actin also contained 0.2 mM ATP and 80 μM $MgCl_2$. (●) MgATP-actin, critical concentration = 0.19 μM (S.D. = ± 0.11 μM, $n = 5$); (○) NFA, critical concentration = 0.06 μM (S.D. = ± 0.04 μM, $n = 5$).

polymerization of MgATP-actin. The slope of pyrene fluorescence *versus* actin concentration is about 10 % lower for NFA than MgATP-actin. The pyrene label may be in a different environment in NFA filaments than MgATP-actin filaments, or a small fraction of the NFA may be denatured.

Filaments of NFA are stable for several days in sucrose at room temperature, but depolymerize completely over several hours ($t_{0.5} \sim 40$ minutes) if

Table 1. Stoichiometry (*n*) of nucleotide per actin monomer

Actin	*n* ATP	*n* ADP	*n* AMP
Native	1.03	0.10	ND
Apyrase-treated	0.01 (±0.02)[a]	0.01 (±0.01)	ND

ND, none detected.
[a] Uncertainties represent ±1 S.D.; *n*=3.

gently diluted tenfold into polymerization buffer without sucrose (Figure 1(b)). This slow time course suggests that filaments do not disassemble catastrophically. Instead they depolymerize slowly from their ends, followed by irreversible denaturation of unstable NFA monomers (De La Cruz & Pollard, 1995). In contrast, when filaments polymerized from ATP-actin are diluted tenfold from 46 % sucrose into polymerization buffer without sucrose, they depolymerize only to the extent required to bring the actin monomer concentration to the critical concentration (Figure 1(b)). The higher fluorescence of a given actin polymer concentration after dilution is due to the quenching of pyrene fluorescence by sucrose (De La Cruz & Pollard, 1995).

The lag phase at the outset of polymerization in KCl is less pronounced for NFA than MgATP-actin (Figure 2). Rapid elongation (~600-2000 seconds of time course) is slower for NFA. The final steady-state fluorescence of NFA is 13 % lower than native actin, in agreement with the 10 % lower slope of fluorescence *versus* polymer concentration in steady-state experiments (Figure 1(a)).

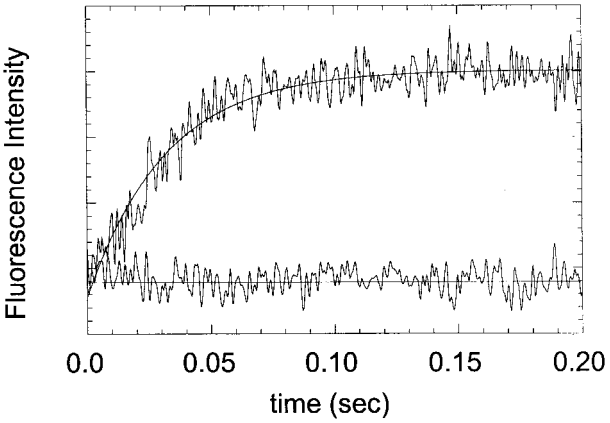

Figure 3. Nucleotide binding to NFA monomers and filaments. Time course of the fluorescence change after mixing 1.5 μM NFA monomers (top) or filaments (bottom) with 10 μM MgεATP. Like NFA filaments, MgATP actin monomers and ADP-actin filaments yielded no fluorescence transients on this time scale. Final conditions: 23 % sucrose, 50 mM KCl, 1 mM EGTA, 10 mM imidazole (pH 7.0), 0.5 mM DTT, 25 °C.

Ligand binding by nucleotide-free actin (NFA) filaments

NFA monomers bind εATP rapidly but NFA filaments do not (Figure 3). Nucleotide-free filaments bind εATP at least 1000 times slower than NFA monomers. MgATP monomers bind εATP at an intermediate rate owing to slow dissociation of the bound nucleotide (Kinosian *et al.*, 1993; De La Cruz & Pollard, 1995), while ADP-actin filaments exchange nucleotide slowly if at all (Pollard *et al.*, 1992). Time courses of 10 μM MgεATP binding to NFA monomers follows single exponentials with rates of 32.1 (±1.4) s^{-1}, yielding a second-order association rate constant of 3.2 μM^{-1} s^{-1} for binding to NFA monomers in 25 % sucrose, in agreement with our earlier measurements (De La Cruz & Pollard, 1995).

NFA filaments bind phalloidin slower ($k_+ = 1.0$ (±0.1) × 10^4 M^{-1} s^{-1} in 11 % sucrose) than ADP-actin filaments ($k_+ = 1.4$ (±0.1) × 10^4 M^{-1} s^{-1}; Figure 4). The fluorescence enhancement of rhodamine phalloidin bound to NFA is ~1.4 times greater than with filaments containing bound nucleotide (Figure 4(a)). Phalloidin dissociates at essentially the same rate from both actins (NFA = 3.8 (±0.2) × 10^{-4} s^{-1}, MgADP-actin = 3.4 (±0.2) × 10^{-4} s^{-1}). The equilibrium binding affinity determined from the ratio of rate constants is 38 (±4) nM for NFA and 24 (±4) nM for ADP-actin filaments (De La Cruz & Pollard, 1996; Allen *et al.*, 1996). By fluorescence microscopy NFA filaments stained with rhodamine phalloidin are similar to filaments polymerized from MgATP actin (not shown).

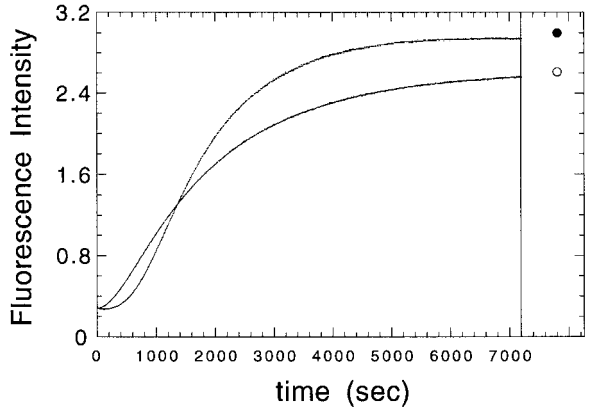

Figure 2. Spontaneous polymerization of MgATP actin and NFA monomers. Polymerization was measured from the fluorescence of 4.5 μM pyrene-actin after addition of KCl. Final conditions are the same as for Figure 1(a). MgATP-actin also contains 0.2 mM ATP and 80 μM $MgCl_2$.

Electron microscopy of nucleotide-free actin (NFA) filaments

By visual inspection of negatively stained specimens (Figure 5) viewed at 30,000× (by CTEM) and 500,000× (by STEM) NFA filaments are morphologically similar to ADP-actin filaments. Quantitative analysis of the images revealed small but statistically significant differences in polymer stiffness and subunit shape. The best data came from comparing phalloidin-stabilized NFA and ADP-actin filaments. Without phalloidin, few NFA and ADP-actin filaments adhered to the grids in the presence of sucrose, even though SDS-PAGE of

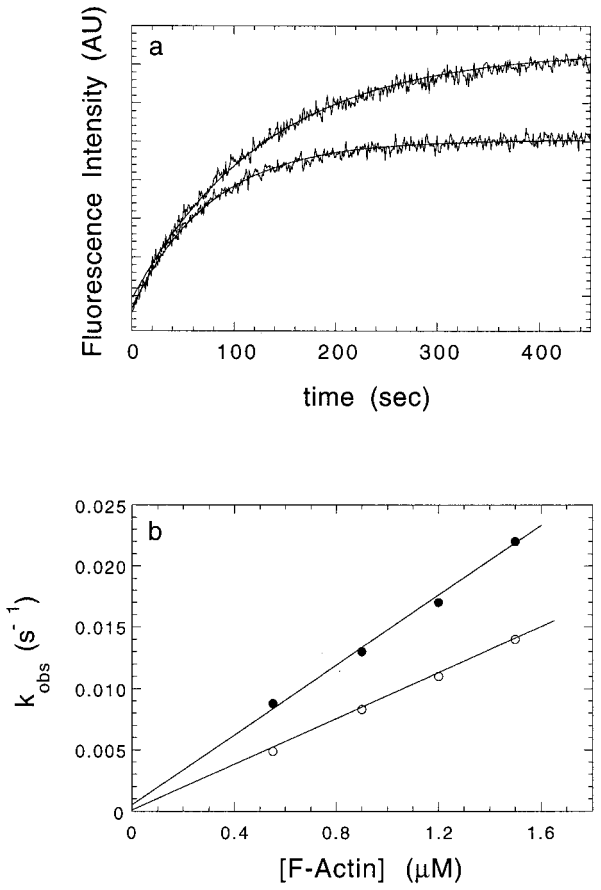

Figure 4. Rhodamine phalloidin binding to NFA filaments. (a) Time course of the fluorescence change after mixing 0.9 μM filaments assembled from MgATP-actin (bottom) or NFA (top) with 40 nM rhodamine phalloidin. The continuous lines are the best fits to single exponentials. (b) Dependence of k_{obs} on [actin]. The second-order association rate constants for rhodamine phalloidin binding are 1.4 (±0.1) × 10^4 M^{-1} s^{-1} for MgATP actin and 1.0 (±0.1) × 10^4 M^{-1} s^{-1} for NFA filaments. Final conditions: 11 % sucrose, 50 mM KCl, 1 mM EGTA, 10 mM imidazole, 0.5 mM DTT, 25 °C. MgATP-actin also contains 0.2 mM ATP and 80 μM $MgCl_2$.

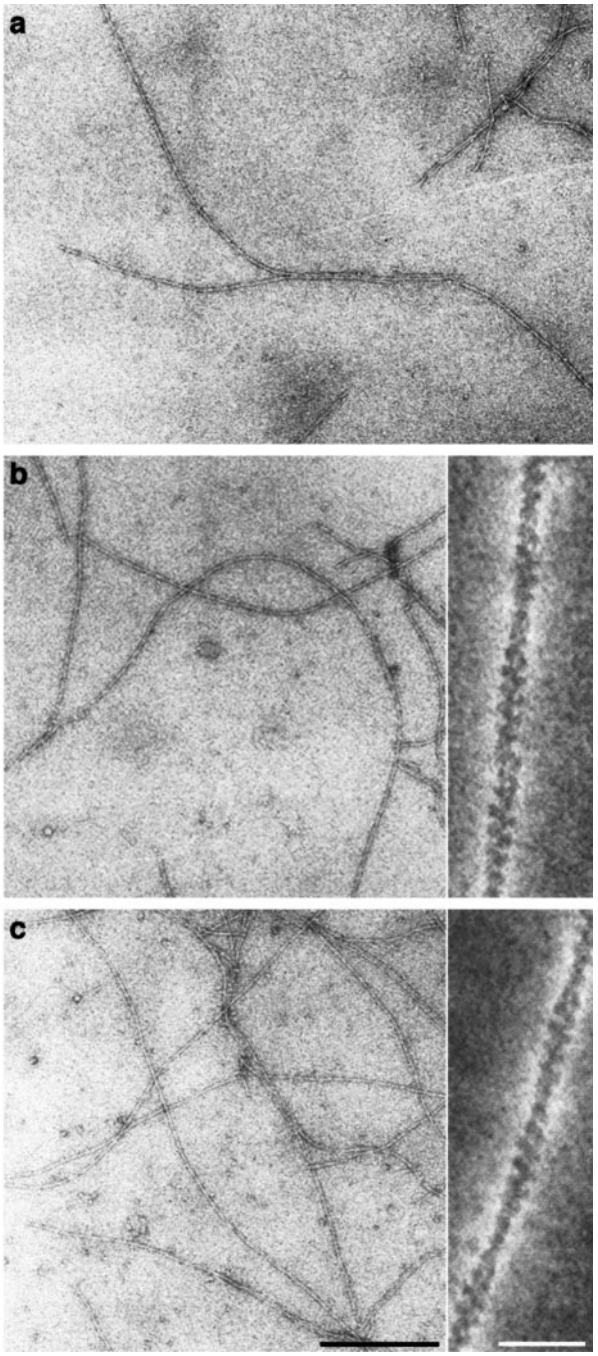

Figure 5. Electron micrographs of negatively stained actin filaments. Negatively stained (a) NFA filaments (in 50 % sucrose), (b) phalloidin-stabilized NFA filaments, and (c) phalloidin-stabilized ADP-actin filaments imaged by CTEM at a nominal magnification of 30,000× (overviews) and by STEM at a nominal magnification of 500,000× (insets). The scale bars represent 250 nm (overviews), and 20 nm (insets).

centrifuged samples confirmed that essentially all of the actin was polymerized (not shown; Figure 1). With phalloidin large numbers of filaments adhered to the grids making it possible to evaluate at least 150 filaments to determine small structural differences between the preparations.

We evaluated filament stiffness by measuring persistence lengths (Table 2), a statistical relationship between the end-to-end distance (R) and the contour length (L) of a filament or filament segment (Orlova & Egelman, 1993; Steinmetz *et al.*, 1997) according to the relation (Landau & Lifshitz, 1958):

$$\langle R^2 \rangle = 2\lambda^2(L/\lambda - 1 + e^{-L/\lambda})$$

Stiffer filaments have longer persistence lengths. Phalloidin-stabilized NFA filaments reveal a larger persistence length than phalloidin-stabilized ADP-actin filaments (Table 2). ADP-actin filaments without phalloidin have even shorter persistence lengths. Other parameters including helical screw

Table 2. Structural and mechanical parameters of actin filaments

Condition	Helical screw angle (°)	Crossover spacing (nm)	Max. crossover width (nm)	Radius of gyration (nm)	Persistence length (μm)
NFA (+Ph)	−167.4	38.6 ± 4.6	8.5 ± 0.9	2.40 ± 0.16	8.0 ± 0.7
Control (+Ph)[a]	−166.9	37.0 ± 2.6	8.5 ± 0.7	2.43 ± 0.06	5.2 ± 0.8
Control (−Ph)[a]	−166.2	35.1 ± 2.0	9.7 ± 0.5	2.51 ± 0.90	2.9

[a] Values are from Steinmetz *et al.* (1997).

angles, radius of gyration, crossover spacings and maximum crossover widths are similar for NFA and ADP-actin filaments (Table 2), indicating that neither bound nucleotide nor phalloidin alter the overall structure of the filament.

However, 3-D helical reconstructions revealed a small localized difference in mass density of NFA filaments relative to ADP-actin filaments (Figure 6). STEM annular dark-field (ADF) images of negatively stained specimens (Figure 5(b) and (c); high-magnification views) were used to generate 3-D helical reconstructions at a nominal resolution of 2.5 nm. Surface rendering of the data contoured to include 100 % of the nominal mass (Figure 6(b)) emphasizes the intersubunit contacts along and between the two

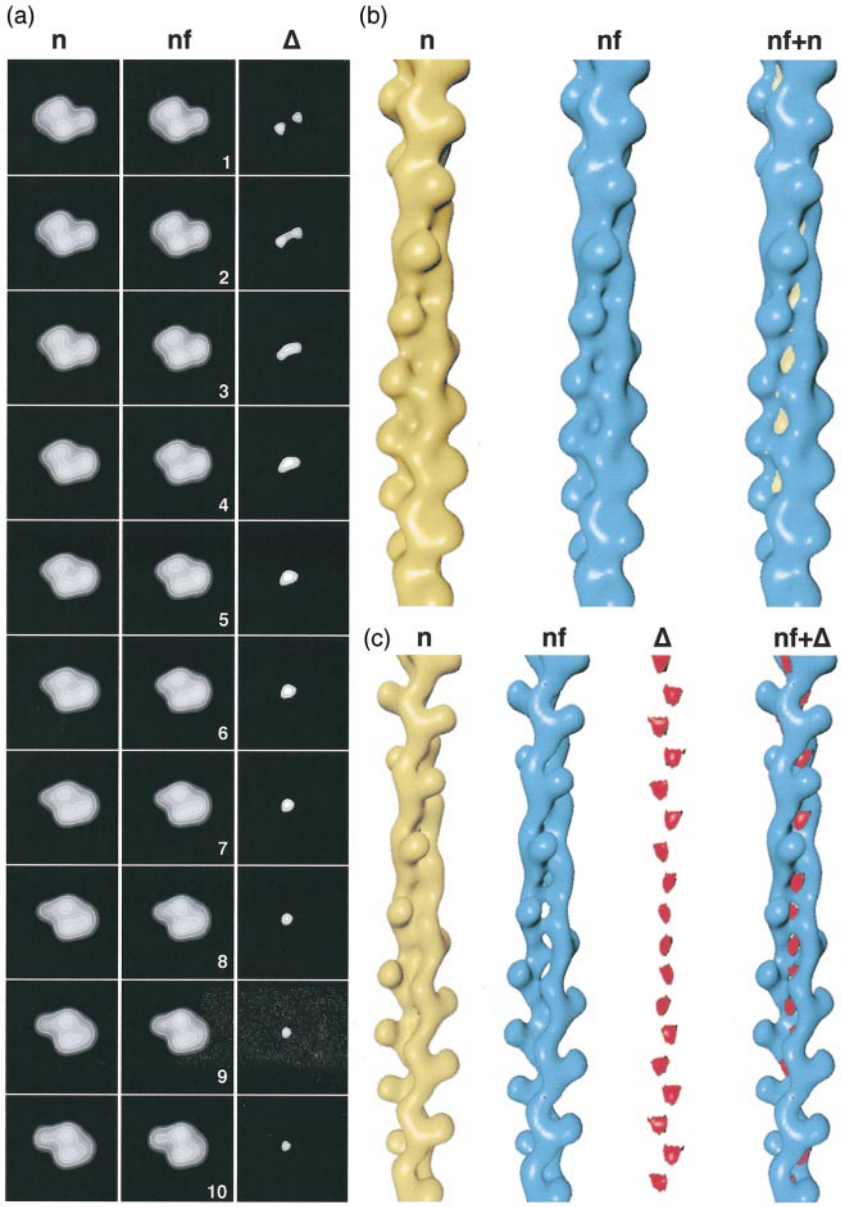

Figure 6. Three-dimensional reconstruction of NFA filaments. Refined and averaged 3-D reconstructions at a nominal resolution of 2.5 nm are displayed as (a) 2.75 Å spaced sections normal to the filament axis with superimposed contours and surface-rendered to include (b) 100 % or (c) 30 % of their nominal molecular volume. The ten sections in (a) represent one axially repeating unit of 2.75 nm of the left-handed genetic helix. The difference map (△) in (a) was calculated by subtracting, section by section, the averaged phalloidin-stabilized NFA filament 3-D reconstruction (nf) from the averaged phalloidin-stabilized ADP-actin filament 3-D reconstruction (n). The resulting image was contrast adjusted (i.e. by ''top/bottom'' slicing) so as to only display the intensities with a >99 % confidence level (Steinmetz *et al.* 1998). Whereas the map (nf + n) in (b) was generated by superimposing the nucleotide-containing reconstruction onto the nucleotide-free reconstruction, the difference map (△) in (c) was generated using the calculated difference maps obtained from the individual sections (△ in (a)).

long-pitch helical strands (Bremer *et al.*, 1994; Steinmetz *et al.*, 1997) and indicates a subtle difference between NFA and ADP-actin filaments. Superimposing the two reconstructions reveals a single contiguous surface pad in the groove between the two long-pitch helical strands where the mass density of ADP-actin filaments bulges out of the NFA filament contour (Figure 6(b); nf + n). Hence, NFA subunits are slightly more compact than ADP-actin subunits. This difference can be seen more clearly by contouring the reconstruction so as to include 30 % mass (Figure 6(c)), which reveals an attenuated mass density between the two long-pitch helical strands of NFA filaments. Subtracting the 30 % mass-contoured NFA filament reconstruction from the ADP-actin filament reconstruction yields a single positive difference peak between actin subunits in opposite long-pitch helical strands (Figure 6(c)). This difference corresponds to the reduction in mass density between the two long-pitch helical strands of NFA filaments. The ''holes'' in the lateral contacts do not coincide with the phalloidin binding site (Steinmetz *et al.*, 1998), or with the vacated nucleotide binding pocket of the nucleotide-free F-actin subunits. In contrast, the mass densities along the two long-pitch helical strands (longitudinal contacts) are practically indistinguishable when contoured to include 30 % mass (Figure 6(c)) just as they were at 100 % (Figure 6(b)), suggesting that the longitudinal intersubunit contacts are not significantly affected by the absence of the high-affinity nucleotide.

Discussion

Although chelation of divalent cations with EDTA substantially reduces the affinity of actin for ATP and ADP, cation-free actin binds these nucleotides strongly enough to compete effectively with Dowex-1. Hence, treatment of actin with EDTA and Dowex-1 removes only 80 % of the bound nucleotide (De La Cruz & Pollard, 1995). Apyrase dephosphorylates free ATP and ADP to AMP, which has such a low affinity for actin that virtually all of the nucleotide dissociates. Kasai *et al.* (1965) used urea to reduce the affinity of actin for ATP.

We confirm the observation of Kasai *et al.* (1965) that NFA polymerizes in KCl and show that the critical concentration is lower than for MgATP-actin (Figure 1). This strong tendency to polymerize is also seen in the assembly of NFA at room temperature in low ionic strength monomer buffer. The low critical concentration of NFA may be related to closure of the nucleotide cleft during polymerization. Sucrose stabilizes NFA monomers with a partially open cleft (De La Cruz & Pollard, 1995). In the absence of sucrose, this conformation is unstable so NFA denatures rapidly and irreversibly. Since the nucleotide cleft is closed in filaments, water is probably released from the cleft during polymerization, as during the closure of the homologous nucleotide binding cleft in hexokinase (Reid & Rand, 1997). This dissociation of water may favor polymerization relative to MgATP-actin, where the cleft is closed in both monomer and polymer (Wriggers & Schulten, 1997) and sucrose does not affect polymerization (Drenckhahn & Pollard, 1986; Fuller & Rand, 1999). Quantitative determination of the number of dissociating water molecules is complicated by the irreversible denaturation of NFA monomers without high sucrose (De La Cruz & Pollard, 1995).

The lag phase during spontaneous polymerization is shorter for NFA than MgATP-actin (Figure 2). This may reflect the tendency of NFA to polymerize even in low salt at 25 °C or to form more stable oligomers. Although stable in sucrose, when diluted into a low sucrose concentration, NFA filaments eventually depolymerize, because subunits dissociating from the filaments rapidly denature. Thus, bound nucleotide is not required directly either to form an actin filament or to maintain its integrity.

NFA filaments appear slightly less massive than ADP-actin filaments (Figure 6). The reorganized mass gives rise to distinct ''holes'' in the groove between the two long-pitch helical strands of subunits (Figure 6(c)). This reorganization, however, does not appear to correspond to a simple rocking motion of the two halves of the protein to close the nucleotide cleft. Rather, when compared with ADP-actin filaments (Figure 7), the major difference peak of NFA filaments is near but does not coincide with the vacated nucleotide binding site which, in turn, is no longer accessible to free nucleotide in the solution. In contrast, the mass density and intersubunit contacts along the two long-pitch helices appear indistinguishable in ADP-actin and NFA filaments (Figure 6(c), n and nf).

NFA monomers but not filaments bind nucleotide rapidly (Figure 3). Even though the nucleotide binding site in filaments is vacant, it is inaccessible to free nucleotide in the solvent. In this respect NFA filaments appear to be similar to ADP-actin filaments in that they do not bind nucleotide from the medium. However, the reason may differ. The exchange of ADP bound to actin filaments with free nucleotide is presumed to be due to the slow dissociation of the bound ADP from the filaments. The new results suggest that even an empty nucleotide binding site in filaments is inaccessible to free nucleotide, presumably because the cleft is partially closed.

Rhodamine phalloidin binding to NFA filaments differs in two ways from ADP-actin filaments: binding is slower and the final fluorescence is 1.4 times higher. Thus, the absence of nucleotide must change the conformation around the phalloidin binding site. The observed changes in twist (Table 2) may be partially responsible for the slower phalloidin binding kinetics, and since the rate of phalloidin binding is determined by the

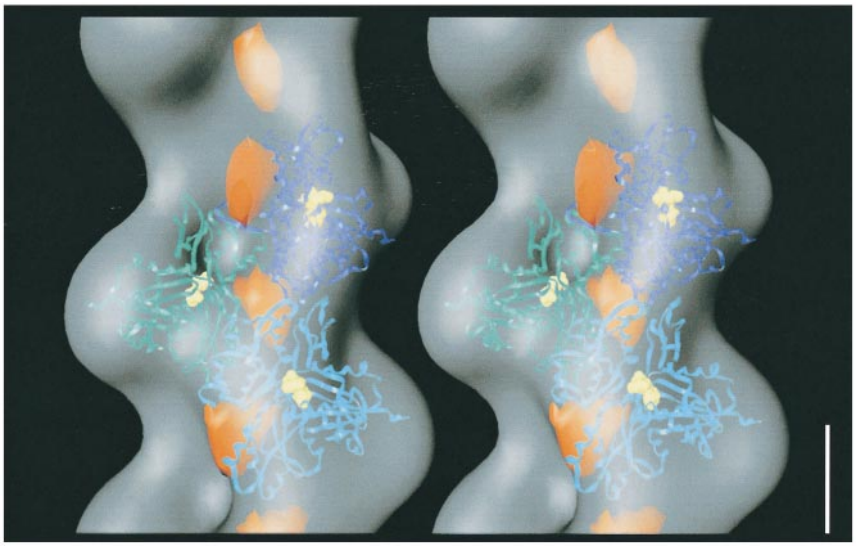

Figure 7. Mapping the major difference peak between ADP-actin filaments and NFA filaments relative to the ''Holmes-Lorenz'' atomic model of the actin filament. For alignment of the atomic model of the F-actin filament relative to the EM-based NFA filament 3-D reconstruction (Figure 6 (nf)), an electron density map was computed from the atomic coordinates of the phalloidin-stabilized F-actin trimer (Lorenz *et al*., 1993) at 25 Å resolution and surface-rendered so as to include 100 % of its nominal mass. The thus represented ''Holmes-Lorenz'' model was then interactively fitted into a semi-translucent surface representation of the EM-based 3-D filament reconstruction and, upon proper alignment, replaced by a ribbon representation with the three actin subunits colored in green, blue and cyan, and the nucleotide residing in its high-affinity site in yellow. The major difference peak between ADP-actin filaments and NFA filaments (i.e. as represented in Figure 6(b), (nf+n) and (c) (△)) was placed into the 3-D scene and colored in orange.

conformational dynamics and subunit flexibility of the polymer (''filament breathing'' model described by De La Cruz & Pollard, 1996; Allen *et al*., 1996), slower binding may also reflect a less dynamic filament, as also indicated by the greater persistence length (Table 1).

Our results show that bound ATP and its hydrolysis in actin filaments are useful kinetically, but not required thermodynamically for assembly of stable filaments. The low critical concentration suggests the NFA subunits dissociate very slowly from the ends of actin filaments. Without bound nucleotide, the polymer cannot take advantage of ATP hydrolysis and phosphate dissociation to provide the energy for different critical concentrations at the two ends (which drives subunit flux) or for the conversion of slowly dissociating ATP-subunits into rapidly dissociating ADP-subunits, which is presumed to prepare filaments for rapid disassembly subsequent to their assembly (discussed in detail by Pollard, 1986). ATP hydrolysis and phosphate dissociation regulate the dynamics and mechanical properties of actin filaments and may also provide an intrinsic timer that controls the interaction of filaments with regulatory proteins, such as members of the cofilin/ADF family (Maciver *et al*., 1991).

Materials and Methods

Reagents

Salts, buffers, chemicals, fluorescence grade imidazole, grade I adenosine 5′-triphosphate (ATP) and grade VII potato apyrase were from Sigma Chemical Co. (St. Louis, MO). Sucrose (Ultra Pure) came from GIBCO BRL (Gaithersburg, MD). Dowex AG 1-X2 and AG 1-X4 resin was from BioRad (Hercules, CA). Pyrenyliodoacetamide, εATP and rhodamine phalloidin were from Molecular Probes (Eugene, OR), DNase I was from Boehringer-Mannheim (Indianapolis, IN) and DNase I beads were prepared as described (Cook & Rubenstein, 1992).

Protein purification and modification

Actin was purified from rabbit skeletal back and leg muscles with an additional gel filtration step (MacLean-Fletcher & Pollard, 1980) over Sephadex G-150 or Sephacryl S-300 equilibrated with buffer A (0.2 mM ATP, 0.5 mM DTT, 0.1 mM $CaCl_2$, 1 mM NaN_3, 2 mM Tris (pH 8.0)) at 4 °C. Actin concentration was determined by absorbance at 290 nm using a molar extinction coefficient of 2.66×10^4 M^{-1} cm^{-1} (Houk & Ue, 1974). Actin was labeled on C374 with pyrene-iodoacetamide (Pollard, 1984), gel filtered and used at 100 % or 5 % of the total actin concentration. Mg-actin was made from Ca-actin in buffer A by addition of 50-80 μM Mg and 200 μM EGTA three to five minutes prior to use as suggested by Kinosian *et al*. (1993).

Preparation of nucleotide-free actin

NFA was prepared by mixing 250 μl of CaATP G-actin treated twice with Dowex to remove free nucleotides and 850 μL of ice-cold S-buffer (1 g sucrose plus 750 μl of 20 mM Tris (pH 8.0)) containing 0.5 mM DTT and 500 μM EGTA or EDTA (to decrease the concentration of free divalent cation and dissociate the bound ATP), equilibrating on ice for five minutes, then treating with 20 units/ml apyrase for 60 minutes on ice. The final sucrose concentration is calculated to be 51 % (w/v). In control samples the five minute preincubation with EDTA was omitted, 20 mM Tris buffer (pH 8.0), was substituted for apyrase, ATP and EGTA were added to 200 μM and $MgCl_2$ to 50-80 μM. This yields a solution of MgATP-actin in 51 % sucrose.

Determination of nucleotide bound to actin

To determine the nucleotide bound to monomers 600 µl of 1.5 µM apyrase-treated or control actin was mixed with 200 µl packed DNase I beads and rocked at 4 °C (Rosenblatt *et al.*, 1995). After 60 minutes the DNase I beads containing actin and bound nucleotide were pelleted at 14,000 *g*. ATP-actin and apyrase-treated actin bind DNase beads equally. Beads with bound actin were washed three times with 1 ml ice-cold 20 mM Tris (pH 8.0), suspended in 300 µl of Tris buffer and boiled for five to ten minutes in a water bath. Boiling denatures the actin and releases the bound nucleotides. The beads were removed by centrifugation and nucleotide separated from denatured actin by passage through a 10,000 MWCO filter (Millipore, Ultra-free MC). The filtrate contains nucleotide released from actin. The composition of the bound and free fractions were determined by HPLC (see below).

HPLC analysis of nucleotides

Nucleotide composition was determined with a Waters model 510 HPLC equipped with a Dupont Zorbax SAX Biocolumn (6.2 mm × 8 cm; PN 820944.903) equilibrated in 0.1 M NH_4HCO_3 (pH 7.5). Samples were applied to the column in 0.2 ml volumes, eluted with a linear gradient of 0.1 M to 0.5 M NH_4HCO_3, and detected at 259 nm with a Waters model 441 absorbance detector. The flow rate was 1 ml/minute. Nucleotide concentrations were calculated from peak areas using known concentrations as standards.

Polymerization and determination of critical concentration

Steady-state polymerization was assayed from the fluorescence intensity ($\lambda_{ex} = 365$ nm, $\lambda_{em} = 407$ nm) of samples containing a 5 % pyrenyl-actin. NFA was polymerized with 0.1 volume of 10 × KEI (500 mM KCl, 10 mM EGTA, 100 mM imidazole (pH 7.0)). Control ATP-actin was polymerized the same way except 200 µM ATP and 80 µM $MgCl_2$ were included to prevent dissociation of the bound nucleotide. Stock polymer solution was diluted with the corresponding polymerization buffer to a range of actin concentrations, sonicated briefly in a bath sonicator, incubated at 22 °C for two to eight hours before recording steady-state fluorescence intensities. Polymerization was confirmed by viscometry with an Ostwald capillary viscometer size 150 (Cannon Instrument Company, College Park, PA). The sample volume was 900 µl. Viscometers were calibrated with buffer lacking actin.

Polymerization kinetics were measured from the fluorescence of pyrene-labeled actin (100 %). All fluorescence measurements were made at 25 °C with a PTI Alphascan fluorescence spectrophotometer.

Ligand binding kinetics

The rates of nucleotide binding were determined from the fluorescence change of εATP after mixing 3 µM actin monomers or filaments in 46 % sucrose buffer containing no free nucleotide with an equal volume of 20 µM MgεATP in buffer containing no sucrose at 25 °C using a stopped-flow apparatus as described (De La Cruz & Pollard, 1995).

Phalloidin binding was assayed by the fluorescence enhancement ($\lambda_{ex} = 550$ nm, $\lambda_{em} = 575$ nm) of rhodamine phalloidin (De La Cruz & Pollard, 1996) after mixing filaments assembled in sucrose with rhodamine phalloidin in polymerization buffer containing no sucrose. The second-order association rate constants were determined from the concentration dependence of the observed rates on actin filament concentration. Dissociation was measured after mixing rhodamine phalloidin labeled filaments with an excess of unlabeled phalloidin (De La Cruz & Pollard, 1996). Final conditions were 11 % sucrose, 40 nM rhodamine phalloidin and the indicated actin concentrations, 25 °C. Filaments with bound rhodamine phalloidin were visualized on a Leica DM IRB fluorescence microscope.

Electron microscopy and image analysis

Nucleotide-free (NF) and nucleotide-containing (N) EGTA-actin were polymerized with 100 mM KCl and equilibrated at room temperature for one hour, either in the absence or presence of two molar equivalents of phalloidin. The sample was centrifuged for 15 minutes at 100,000 *g* and the pelleted material was resuspended in an initial volume of polymerization buffer without sucrose (100µl). A 5 µl aliquot was immediately applied to a glow-discharged, carbon-coated 400 mesh/inch copper grid and allowed to adsorb for 60 seconds (NFA filaments) or 30 seconds (EGTA-actin filaments). Excess liquid was removed by blotting and the grid was washed on several drops of water before negatively staining with 0.75 % (w/v) uranyl formate. For low-magnification overviews and persistence length measurements, specimens were examined and imaged with a Hitachi CTEM H-7000 (Tokyo, Japan) conventional transmission electron microscope (CTEM).

High-magnification annular dark-field (ADF) images of the same negatively stained samples were recorded digitally in a scanning transmission electron microscope (STEM) (STEM HB5; Vacuum Generators, East Grinstead, England) and used for quantitative structural analysis and 3-D helical reconstruction (Steinmetz *et al.*, 1997). Briefly, about 150 filament stretches, each 100-200 nm long, were digitally straightened using the SEMPER6 image processing package (Saxton, 1996). The straightened filament stretches were subjected to 3-D helical reconstruction using the Micrograph Data Processing Program MDPP (Smith & Gottesman, 1996). Filament segments consisting of two helical repeats (i.e. two crossovers of the two long-pitch helical strands) were D(Z,k)-filtered (Smith & Aebi, 1974) employing the integer helical selection rule $l = -7n + 15\ m$ (screw angle $\Psi = -168.0°$), whereby the helical repeat length and radial position of the filament axis were optimized *via* a 3-D helical parameter search (Bremer *et al.*, 1994). The ten filaments with the highest transmitted power upon D(Z,k)-filtration were Fourier-transformed, and their equator, the 1st, 2nd, 6th, 7th, 8th, 9th, 15th and 16th layerlines extracted. Layerline correlation with a reference was used to align and average a set of D(Z,k)-filtered and layerline-extracted filament segments (Smith *et al.*, 1976). The 3-D reconstructions were computed (DeRosier & Moore, 1970; Smith *et al.*, 1976) and surface-rendered by isocontouring them with a program implemented on a Silicon Graphics (Mountain View, CA) computer (Henn *et al.*, 1996). Contouring levels were selected to include the nominal

molecular volume of the 43 kDa actin subunit or fractions of it, taking into consideration the calculated cylindrical radius of gyration of the respective reconstructions.

Acknowledgments

This work was supported by NIH research grant GM26338 to T.D.P., an NSF Predoctoral Fellowship Award to E.M.D.L.C., and by the M.E. Müller Foundation of Switzerland and the Canton Basel-Stadt to A.M., M.O.S., D.S. and U.A.

References

Allen, P. G., Shuster, C. B., Kas, J., Chaponnier, C., Janmey, P. A. & Herman, I. M. (1996). Phalloidin binding and rheological differences among actin isoforms. *Biochemistry,* **35**, 14062-14069.

Asakura, S. (1961). The interaction between G-actin and ATP. *Arch. Biochem. Biophys.* **92**, 140-149.

Bremer, A., Henn, C., Goldie, K. N., Engel, A., Smith, P. R. & Aebi, U. (1994). Towards atomic interpretation of F-actin filament three-dimensional reconstruction. *J. Mol. Biol.* **242**, 683-700.

Carlier, M.-F. (1990). Actin polymerization and ATP hydrolysis. *Adv. Biophys.* **26**, 51-73.

Carlier, M.-F. & Pantaloni, D. (1988). Binding of phosphate to F-ADP-actin and role of F-ADP-Pi-actin in ATP-actin polymerization. *J. Biol. Chem.* **263**, 817-825.

Cook, R. K. & Rubenstein, P. A. (1992). In *The Cytoskeleton: A Practical Approach* (Carraway, K. L. & Carraway, C. A. C., eds), pp. 99-122, Oxford University Press, New York.

De La Cruz, E. M. & Pollard, T. D. (1995). Nucleotide-free actin: stabilization by sucrose and nucleotide binding kinetics. *Biochemistry,* **34**, 5452-5461.

De La Cruz, E. M. & Pollard, T. D. (1996). Kinetics and thermodynamics of phalloidin binding to actin filaments from three divergent species. *Biochemistry,* **35**, 14054-14061.

DeRosier, D. & Moore, P. B. (1970). Reconstruction of three-dimensional images from electron micrographs of structures with helical symmetry. *J. Mol. Biol.* **52**, 355-369.

Drenckhahn, D. & Pollard, T. D. (1986). Elongation of actin filaments is a diffusion-limited reaction at the barbed end and is accelerated by inert macromolecules. *J. Biol. Chem.* **261**, 12754-12758.

Fuller, N. & Rand, R. P. (1999). Water in actin polymerization. *Biophys. J.* **76**, 3261-3266.

Henn, C., Teschner, M., Engel, A. & Aebi, U. (1996). Real-time isocontouring and texture mapping meet new challenges in interactive molecular graphics applications. *J. Struct. Biol.* **116**, 86-92.

Houk, T. W. & Ue, K. (1974). The measurement of actin concentration in solution: a comparison of methods. *Anal. Biochem.* **62**, 66-74.

Kasai, M., Nakano, E. & Oosawa, F. (1965). Polymerization of actin free from nucleotides and divalent cation. *Biochim. Biophys. Acta,* **94**, 494-503.

Kinosian, H. J., Selden, L. A., Estes, J. E. & Gershman, L. C. (1993). Nucleotide binding to actin. Cation dependence of nucleotide dissociation and exchange rates. *J. Biol. Chem.* **268**, 8683-8691.

Landau, L. D. & Lifshitz, E. M. (1958). *Statistical Physics*, Pergamon, Oxford.

Lorenz, M., Popp, D. & Holmes, K. C. (1993). Refinement of the F-actin model against X-ray fiber diffraction data by the use of a directed mutation algorithm. *J. Mol. Biol.* **234**, 826-836.

Maciver, S. K., Zot, H. G. & Pollard, T. D. (1991). Characterization of actin filament severing by actophorin from *Acanthamoeba castellanii*. *J. Cell Biol.* **115**, 1611-1620.

MacLean-Fletcher, S. & Pollard, T. D. (1980). Identification of a factor in conventional muscle actin preparations which inhibits actin filament self-association. *Biochem. Biophys. Res. Commun.* **96**, 18-27.

Ohm, T. & Wegner, A. (1994). Mechanism of ATP hydrolysis by polymeric actin. *Biochim. Biophys. Acta,* **1208**, 8-14.

Orlova, A. & Egelman, E. H. (1992). Structural basis for the destabilization of F-actin by phosphate release following ATP hydrolysis. *J. Mol. Biol.* **227**, 1043-153.

Orlova, A. & Egelman, E. H. (1993). A conformational change in the actin subunit can change the flexibility of the actin filament. *J. Mol. Biol.* **232**, 334-341.

Pardee, J. & Spudich, J. A. (1982). Mechanism of K^+-induced actin assembly. *J. Cell Biol.* **93**, 648-654.

Pollard, T. D. (1984). Polymerization of ADP-actin. *J. Cell Biol.* **99**, 769-777.

Pollard, T. D. (1986). Rate constants for the reactions of ATP- and ADP-actin with the ends of actin filaments. *J. Cell Biol.* **103**, 2747-2754.

Pollard, T. D. & Cooper, J. A. (1986). Actin and actin-binding proteins. A critical evaluation of mechanisms and functions. *Annu. Rev. Biochem.* **55**, 987-1035.

Pollard, T. D. & Weeds, A. G. (1984). The rate constant for ATP hydrolysis by polymerized actin. *FEBS Letters,* **170**, 94-98.

Pollard, T. D., Goldberg, I. & Schwarz, W. H. (1992). Nucleotide exchange, structure, and mechanical properties of filaments assembled from ATP-actin and ADP-actin. *J. Biol. Chem.* **267**, 20339-20345.

Reid, C. & Rand, R. P. (1997). Probing protein hydration and conformational states in solution. *Biophys. J.* **72**, 1022-1030.

Rosenblatt, J., Peluso, P. & Mitchison, T. J. (1995). The bulk of unpolymerized actin in *Xenopus* egg extracts is ATP-bound. *Mol. Biol. Cell.* **6**, 227-236.

Saxton, O. W. (1996). Semper: distortion compensation, selective averaging, 3-D reconstruction, and transfer function correction in a highly programmable system. *J. Struct. Biol.* **116**, 230-236.

Smith, P. R. & Aebi, U. (1974). Computer generated Fourier transforms of helical particles. *J. Phys. A. Gen. Phys.* **7**, 1627-1633.

Smith, P. R. & Gottesman, S. M. (1996). The micrograph data processing program. *J. Struct. Biol.* **116**, 35-40.

Smith, P. R., Aebi, U., Josephs, R. & Kessel, M. (1976). Studies on the structure of the bacteriophage T4 tail sheath. I. The recovery of 3-D structural information from the extended sheath. *J. Mol. Biol.* **106**, 243-271.

Steinmetz, M. O., Goldie, K. N. & Aebi, U. (1997). A correlative analysis of actin filament assembly, structure and dynamics. *J. Cell Biol.* **138**, 559-574.

Steinmetz, M. O., Stoffler, D., Muller, S. A., Jahn, W., Wolpensinger, B., Goldie, K. N., Engel, A., Faulstich, H. & Aebi, U. (1998). Evaluating atomic

models of F-actin with an undecagold-tagged phalloidin derivative. *J. Mol. Biol.* **276**, 1-6.
Straub, F. B. & Feuer, G. (1950). Adenosine-triphosphate, the functional group of actin. *Biochim. Biophys. Acta*, **4**, 455-470.
Vinson, V. K., De La Cruz, E. M., Higgs, H. N. & Pollard, T. D. (1998). Interactions of *Acanthamoeba* profilin with actin and nucleotides bound to actin. *Biochemistry*, **37**, 10871-10880.
Wriggers, W. & Schulten, K. (1997). Stability and dynamics of G-actin: back-door water diffusion and behavior of subdomain 3/4 loop. *Biophys. J.* **73**, 624-639.

Edited by W. Baumeister

(Received 6 July 1999; received in revised form 10 November 1999; accepted 11 November 1999)